IOP PUBLISHING PLASMA PHYSICS AND CONTROLLED FUSION

Plasma Phys. Control. Fusion **53** (2011) 054002 (11pp) doi:10.1088/0741-3335/53/5/054002

Numerical modelling of electromagnetic turbulent transport of energetic ions in burning plasmas

M Albergante, J P Graves, A Fasoli, M Jucker, X Lapillonne and W A Cooper

Ecole Polytechnique Fédérale de Lausanne (EPFL), Centre de Recherche en Physique des Plasmas, Association EURATOM-Confédération Suisse, 1015 Lausanne, Switzerland

E-mail: mattia.albergante@epfl.ch

Received 16 September 2010, in final form 15 November 2010
Published 31 March 2011
Online at stacks.iop.org/PPCF/53/054002

Abstract

We investigate the redistribution of the neutral beam driven current in the presence of small scale turbulence in the ITER steady-state scenario. Gyrokinetic simulations show that anomalous transport of beam ions can be larger than collisional estimates. The impact on the beam driven current in ITER is studied with a single particle following code. The results indicate that the current driven by the 1 MeV neutral beam injection is not significantly redistributed by the microturbulent fields. The numerical investigation shows that a larger impact is expected for lower energy neutral beams.

(Some figures in this article are in colour only in the electronic version)

1. Introduction

Neutral beam injection (NBI) is envisaged in tokamak experiments to achieve high temperature plasmas and overcome the limitations of Ohmic heating [1]. In addition, neutral beam current drive (NBCD) can be exploited to create an important fraction of non-inductive plasma current. With this method advanced scenarios have been attained in present day tokamaks (see, e.g., [2–5]) and future experiments, such as ITER, rely on the NBI driven current for steady-state operation [6].

The efficiency of the NBI technique for heat deposition and current drive relies on the good confinement of fast ions, whose orbits are determined by plasma equilibrium and electromagnetic perturbations. One possible source of anomalies in the energetic particle trajectories is the interaction with microturbulence. Numerical simulations and theories predicted this interaction [7–9, 10] and experimental confirmations were recently found [11, 12]. These findings demonstrated that turbulent transport is important only for intermediate particle energies, $E \lesssim 10\,T_e$, for passing particles in particular [9, 10, 13]. As plasma heating is provided by particles with higher energy, no significant effects on the heating

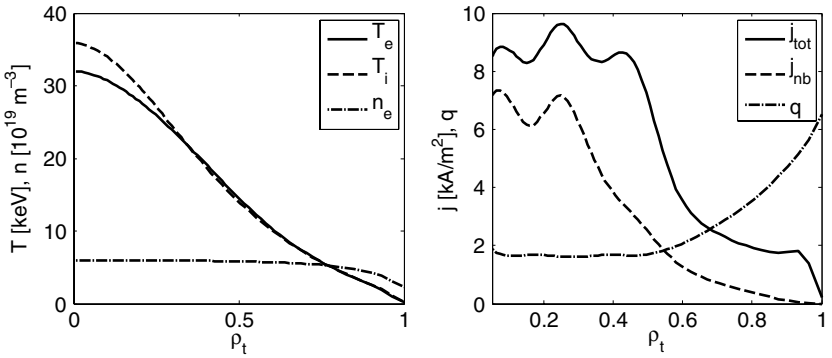

Figure 1. Density and temperature profiles of the background species of an ITER steady-state scenario (left panel). Total current density profile and beam driven fraction as a function of the normalized toroidal flux (right panel). Also shown is the resulting safety factor profile as computed by the CHEASE code [18].

profiles are expected, as demonstrated for alpha particles in recent work [14, 15]. On the other hand, beam particles at intermediate energies could carry an important amount of current and the effect on the NBCD profile needs to be assessed.

In this work we study the redistribution of the NBI driven current in the ITER steady-state scenario due to microturbulence. In section 2 we employ the GENE code [16] to study the linear features of the microturbulence generated by ITER plasmas. A set of parameters for nonlinear analyses is then obtained, and high resolution simulations are performed. These simulations include a population of NBI ions, whose transport is studied in detail. The diffusivity provided by GENE simulations is employed in the numerical NBI model described in section 3, where we focus our analysis on the collisional slowing down of NBI particles with the VENUS code [17]. In section 4 we present the results on the anomalous redistribution of the NBCD profile. The alteration of the beam driven current and the consequential changes in the safety factor are presented and discussed. Conclusions are drawn in section 5.

2. Modelling the microturbulent transport of energetic ions

Several steps are required to reliably describe the small scale turbulence of the ITER steady-state scenario (figure 1). We first study the linear stability of the most important microinstabilities in this plasma configuration. Nonlinear simulations are then required for a thorough description of the turbulent fields affecting the fast ion motion. Both linear and nonlinear simulations are performed by means of the gyrokinetic code GENE [16]. A particularly interesting feature of this code is the possibility of employing the eigenvalue solver in linear simulations [19]. With this numerical module the identification of both dominant and subdominant modes, otherwise challenging with the initial value solver, is straightforward. Nonlinear simulations can then exploit this numerical feature for a first estimate of the time step needed by the Runge–Kutta solver. We employ the local version of the code in the field aligned coordinate system (x, y, z), where x is the normalized toroidal flux, y is a binormal coordinate and z determines the position along the field line. The magnetic configuration of the ITER steady-state scenario is accurately described by the interface with the CHEASE code [18, 20].

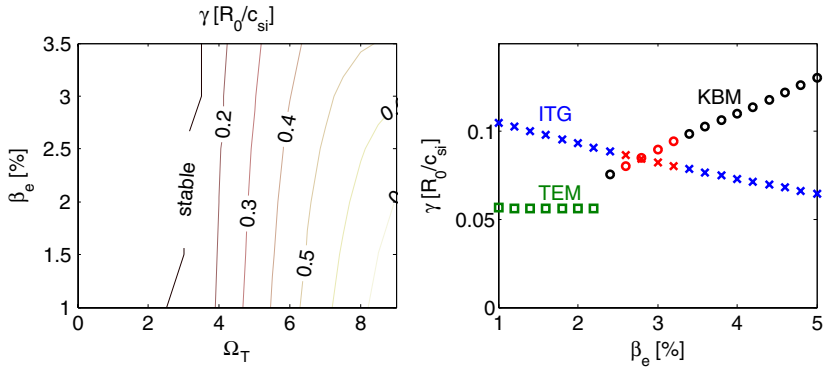

Figure 2. Linear growth rate of the ITG mode as a function of Ω_T and β_e (left panel). The right panel shows the influence of β_e on the three most unstable modes at $\Omega_T = 3.5$. The eigensolver module requires a large number of iterations to converge when different modes are characterized by a similar growth rate. This is the case in the region at $2.4\% < \beta_e < 3.2\%$, where the computational demanding simulations are replaced by interpolated values (red markers).

2.1. Linear simulations with the GENE code

The introductory linear analysis focuses on the influence of two parameters on the growth rate of small scale instabilities. The first parameter is the logarithmic temperature gradient of the background species, defined in GENE as $\Omega_T = -(R_0/a)\,\mathrm{d}\ln T/\mathrm{d}x$, where R_0 and a are the major and minor radius of the tokamak, respectively. The temperature gradient, given the flat density profile characterizing this scenario, is the main instability drive and determines the intensity of the background turbulence. The second parameter is the ratio of the electron pressure to the magnetic pressure. It is defined in the GENE code as $\beta_e = n_e T_e/(B^2_{\rho_t=0.5}/2\mu_0)$ and affects the structure of the microturbulent modes [21]. Furthermore, it determines the strength of magnetic fluctuations, which influences the fast ion motion [9].

We simulate a two species plasma, composed by electrons and deuterium ions at mid-radius $x = 0.5$, focusing our attention on a single mode at $k_y\rho_s \simeq 0.8$. In this definition $\rho_s = c_{s_i}/(eB/m_i)$ is the Larmor radius of the ion species and $c_{s_j} = \sqrt{T_e/m_j}$ (j represents the species index). The two-dimensional scan as a function of Ω_T and β_e is illustrated in figure 2. We observe that the linear growth rate of the internal temperature gradient (ITG) mode is governed by changes in Ω_T, as expected. The ITG branch becomes stable for values of Ω_T below 3, where no other instabilities are present. Also shown is the effect of β_e on the growth rate of the ITG instability. As previously observed in [21, 22], an increase in the electron pressure β_e has a small but beneficial effect on the ITG turbulence. We can also conclude that the turbulence is not affected by the presence of kinetic ballooning modes (KBMs), whose appearance is observed at $\beta_e > 2\%$. For the value of $\beta_e = 1.5\%$ expected for ITER, we note the presence of the trapped electron mode (TEM) for the particular wavenumber considered.

We keep the nominal $\beta_e = 1.5\%$ for this scenario and further investigate the presence of subdominant modes at $\Omega_T = 3.5$, a value close to marginal stability. The analysis is carried out focusing on different wavenumbers k_y. The results of figure 3 reveal the existence of two instabilities. The first corresponds to the aforementioned ITG modes, while the second represents TEMs. Further linear simulations have been performed to clarify the possible presence of electron temperature gradient (ETG) modes. It is found that the largest growth rate of this instability, rescaled to electron units, is much lower than the ITG growth rate at ion

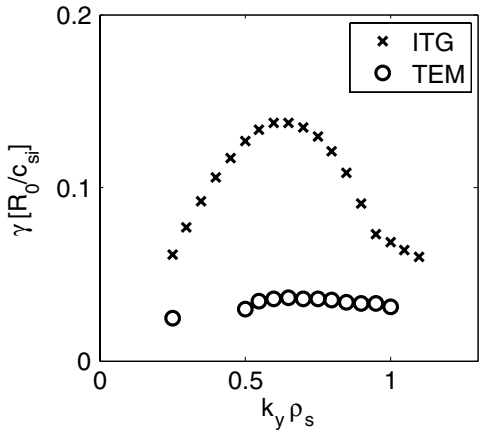

Figure 3. Linear growth rate, as a function of k_y, of the two most unstable modes. The largest γ is found for an ITG mode, with subdominant TEM at similar wavelengths.

scales:

$$\frac{\gamma^{\mathrm{ETG}}}{\gamma^{\mathrm{ITG}}} \ll \sqrt{\frac{m_\mathrm{e}}{m_\mathrm{i}}}. \tag{1}$$

For this reason, only a minor influence of ETG modes on the particle transport is expected [23] and we can neglect them in nonlinear simulations.

2.2. Nonlinear simulations and velocity space investigation with the GENE code

The results of the previous section are now extended to evaluate the transport of NBI ions in ITER. We simulate a two species plasma composed of deuterium and electrons. We set the grid size to $(n_x, n_y, n_z) = (192, 64, 48)$ and $(n_{v_\parallel}, n_\mu) = (64, 32)$. The box size in real space is $(L_x, L_y) = (125, 80)\rho_\mathrm{s}$, and one poloidal turn in z. The extent of the velocity space domain is $(L_{v_\parallel}, L_\mu) = (3v_{\mathrm{th_e}}, 9\,T_\mathrm{e})$. The background species are characterized by similar temperatures ($T_\mathrm{i} = 0.8\,T_\mathrm{e}$), a flat density profile and $\Omega_\mathrm{T} = 3.5$. This value is close to the marginal stability region of the dominant ITG modes. We keep the nominal value of β_e=1.5% in our simulations. A distribution of deuterium ions, in the passive tracer limit, is also included in the simulation. The transport of this population, representative of NBI ions, is evaluated starting from the definition of a *kinetic*, i.e. velocity space dependent, diffusivity [13, 24]

$$D_v(\boldsymbol{v}) = -\frac{1}{\nabla \ln n}\frac{\delta f(\boldsymbol{v})\delta u(\boldsymbol{v})}{f_0(\boldsymbol{v})}. \tag{2}$$

Here, f_0 is a Maxwellian distribution, δf is the perturbation in the distribution function and δu is the perturbed radial particle drift, which can be separated into two components

$$\delta u = \delta u_{E\times B} + \delta u_{A_\parallel} = -\left(\frac{\boldsymbol{\nabla}\delta\bar{\Phi}\times\boldsymbol{B}}{B^2} + v_\parallel\frac{\boldsymbol{\nabla}\delta\bar{A}_\parallel\times\boldsymbol{B}}{B^2}\right)\cdot\hat{\boldsymbol{e}}_r, \tag{3}$$

where an overbar denotes a gyroaveraged quantity. The two terms in the perturbed drift generate the so-called 'electrostatic' and 'magnetic' components of the particle diffusivity. The separation is necessary as the transport features arising from the different perturbed velocities can be rather dissimilar [9].

The results shown in figure 4 demonstrate the existence of turbulent transport of fast ions. The effect is very significant, if we consider that the collisional diffusivity employed in

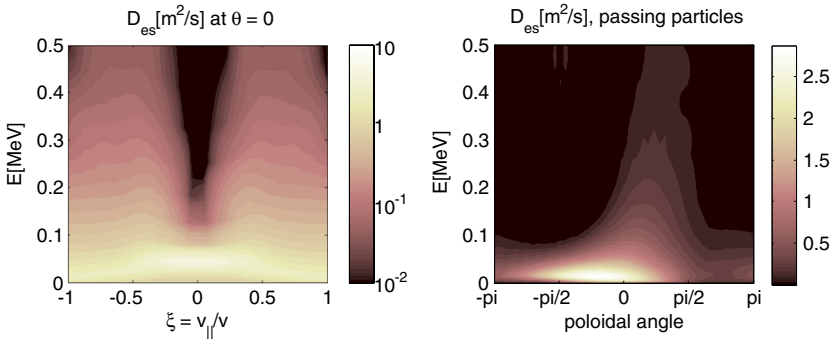

Figure 4. Electrostatic diffusivity, as a function of energy and pitch $\xi = v_\parallel/v$, for particles on the outboard mid-plane (left panel). The particle diffusivity is also shown as a function of energy and poloidal angle for passing particles at $\xi \simeq 1$ (right panel).

predictive models for ITER is of the order of $0.1\,\mathrm{m^2\,s^{-1}}$. This value is exceeded by passing particles at large $|\xi| = |v_\parallel|/v$, which are characterized by fast orbits around the poloidal plane, small unperturbed radial drift and most importantly small Larmor radius. Therefore, the beneficial gyroaveraging effects usually observed for energetic ions are not present. This indicates that before their slowing down is concluded, NBI ion trajectories can be significantly modified by microturbulence. On the other hand, the large Larmor radius of trapped particles effectively suppresses the particle transport as we observe in the $\xi \simeq 0$ region of the plot.

The particle energy and pitch ξ are not the only parameters regulating the intensity of the radial transport. Indeed, the turbulent fields in tokamak geometry exhibit a well-known poloidal dependence. In the outboard mid-plane the instability is the strongest, as expected from the adverse alignment of the curvature drift and the pressure gradient. The energetic ion transport reflects this poloidal asymmetry (figure 4). The short transit time of beam ions, however, may cause these particles to experience only a poloidal average of the particle transport.

The transport of energetic ions due to magnetic fluctuations has also been investigated. It is found that magnetic transport plays only a minor role in this scenario. The electromagnetic contribution to the particle diffusivity (equation (2)), coupled with the perturbed $A_\parallel$ drift, never exceeds $D^{\mathrm{em}} \simeq 10^{-2}\,\mathrm{m^2\,s^{-1}}$, which is small compared with the electrostatic diffusivity $D^{\mathrm{es}} > 10^{-1}\,\mathrm{m^2\,s^{-1}}$. We consequently focus on the electrostatic transport of these particles for the rest of this work.

3. Modelling the NBI

The findings of the previous section demonstrate how under certain conditions the transport of suprathermal populations can exceed collisional values. In this section we evaluate the impact that this phenomenon can have on the key properties of the ITER steady-state scenario plasma. In particular, we are interested in the anomalous redistribution of the NBCD profile and in the consequent modification to the safety factor profile. The shape of the current density is tailored to obtain a flat q profile in the plasma core, where $q(0) = q_{\min} > 1.5$ (figure 1). Electron cyclotron current drive (ECCD), in addition to the bootstrap current, is also used to achieve this goal. This plasma configuration is characterized by a broader MHD stable region in operational space [6]. Unexpected changes in the current profile might alter plasma stability and reduce these advantages.

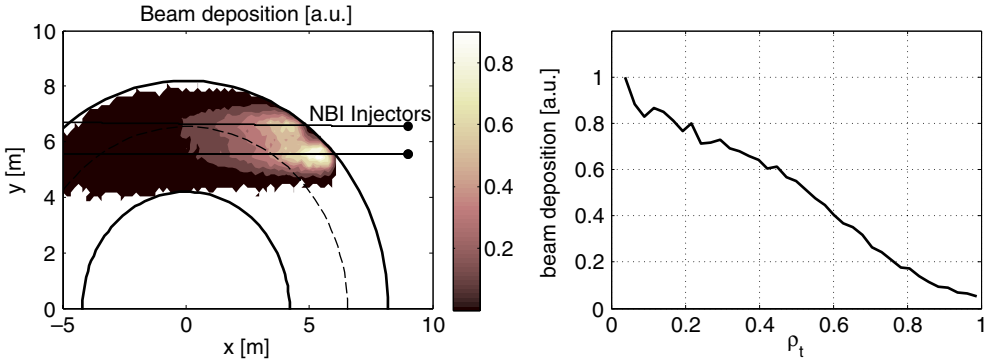

Figure 5. Probability distribution function of ionized NBI particles, as calculated by the model presented in section 3 (left panel). The innermost and outermost position of the plasma column (solid lines) and the magnetic axis are also shown (dashed lines). The corresponding beam deposition profile for this configuration is peaked in the core and rather broad along the radius (right panel).

3.1. Beam ionization model

We model the NBI driven current in the ITER steady-state scenario by first developing a beam ionization model. The intensity of the neutral beam $I(\ell) = N_{\mathrm{b}}(\ell)v_{\mathrm{b}}$, where ℓ is the position along the beam line and v_{b} is the beam velocity, is regulated by the following differential equation [25]:

$$\frac{\mathrm{d}I(\ell)}{\mathrm{d}\ell} = -n_{\mathrm{e}}(\ell)\sigma_{\mathrm{eff}}(\ell)I(\ell). \tag{4}$$

Here, σ_{eff} is an effective cross section embedding several processes that generate ionized particles, such as charge exchange and ionization by background ions and impurities. In our model, we retain the multistep correction to σ_{eff} described in reference [26]. Integrating equation (4) gives

$$I(\ell) = I_0 \mathrm{e}^{-\int_0^{\ell} n_{\mathrm{e}}(\ell')\sigma_{\mathrm{eff}}(\ell')\,\mathrm{d}\ell'}. \tag{5}$$

This equation can be solved numerically once the background plasma profiles and the beam line geometry are known. The detailed geometry of the NBI in ITER is still under development. For this analysis, we model the apparatus as four separate injectors positioned on a square grid whose sides measure 1 m. Each injector consists of a circular source with a beam spread of 1.2°. The injectors are located 9 m away from the tangency point and feed particles to the plasma tangential to the magnetic field (figure 5).

Each numerical particle representative of NBI ions is characterized by three coordinates in real space, two in velocity space and a weight. The real space location of the particles is obtained by uniformly extracting their position along the beam line. To reproduce the collimation of the beam a Gaussian displacement perpendicular to the NBI line is introduced. The injection energy E is equal to 1 MeV. At the same time, we consider minor concentration of particles at fractional energies $E_{\mathrm{nbi}}/2$ and $E_{\mathrm{nbi}}/3$. The pitch of the jth particle can be calculated from the following expression:

$$\xi_j = v_{\parallel_j}/v_j = \boldsymbol{v}_j(\boldsymbol{x}_j) \cdot \frac{\boldsymbol{B}(\boldsymbol{x}_j)}{||\boldsymbol{B}(\boldsymbol{x}_j)||}. \tag{6}$$

The weight assigned to each particle is proportional to the NBI ionization. It is calculated from equation (5) by interpolating the plasma density and temperature profiles from figure 1 along

the beam line. The beam particle deposition for this particular configuration is illustrated in figure 5. Such a broad deposition profile results from the flat density profile characterizing ITER. This feature causes a good fraction of the beam to become ionized far from the core. The beam deposition peaking in the core arises as a consequence of the tangential injection.

A final consideration can be made about the expected beam driven current. The pitch angle of the injected ions is distributed in a narrow region between $\xi = 0.8$ and $\xi = 1.0$. The driven current profile is therefore similar to that of the beam deposition profile. We also expect the collisional relaxation of the deposited current to be small, as the beam particle orbits change significantly only at low energies, where particles provide only small contributions to the current.

3.2. Collisional slowing down of NBI particles

The trajectories of the NBI particles created with the beam ionization model are evolved with the drift kinetic code VENUS [17]. The beam injection is modelled in the code by first defining a time T for the simulation, typically longer than the beam slowing down time. This period T is then divided into M intervals when a number N/M of particles are added to the simulation. By the end of the simulation, a total number of N beam ions are simulated. These particles are tracked until full slowing down, i.e. when their energy is lower than $2\,T_e$. Stationary conditions are reached when the energy given to the background plasma is balanced by the energies of the injected particles.

The VENUS code simulates the motion of the high energy particles subject to unperturbed drifts and to collisions with background species. The collision operator provides the Monte-Carlo scattering of particles in velocity space [27]. To further benchmark this numerical module we build two plasma scenarios for testing purposes. Energetic particles of the first scenario are characterized by a large injection energy $E_b = 40E_c$. The critical energy E_c represents the boundary between electron heating ($E > E_c$) and ion heating ($E < E_c$). The stationary distribution function of the energetic ion population is a slowing down function

$$f_b(E) \propto \frac{1}{E^{3/2} + E_c^{3/2}} \simeq E^{-3/2} \qquad E \gg E_c. \tag{7}$$

We also inject a second population of energetic ions at $E_b = 4\,E_c$. This time we inject the numerical particles at the beginning of the simulation and we track their slowing down until thermal values. The mean energy of such a population, as a function of time, is given by [25]

$$\langle E\rangle(\hat{t}) = E_0[e^{-3\hat{t}} - (E_c/E_b)^{3/2}(1 - e^{-3\hat{t}})]^{2/3}. \tag{8}$$

In this definition we used a normalized time $\hat{t} = t/\tau_e$, where τ_e represents the electron slowing down time and is equal to 3.9×10^{-2} s. The results for the two simulations are illustrated in figure 6. We find a good agreement between the theoretical predictions and the numerical simulation in both cases. The decay of the averaged energy of the distribution shows some disagreement at low values of $\langle E\rangle$, where the validity of equation (8) is questionable. The agreement between the analytical and the simulated slowing down time of the energetic population, $\tau_s = 2.8 \times 10^{-2}$ s, is evident from the figure.

We now employ the NBI distribution obtained with the beam ionization technique and we calculate the stationary distribution function under the influence of Coulomb collisions. We follow the motion of a population of 2.4×10^5 particles for 2 s. The resulting distribution function in velocity space, together with the stationary current profile, is shown in figure 7. The initial distribution of particles is injected in a narrow region of velocity space at high energies and $\xi \simeq 1$. Close to the birth energy, the ions give their energy to the background electrons. This process reduces the energy of the beam particles without notably affecting their pitch

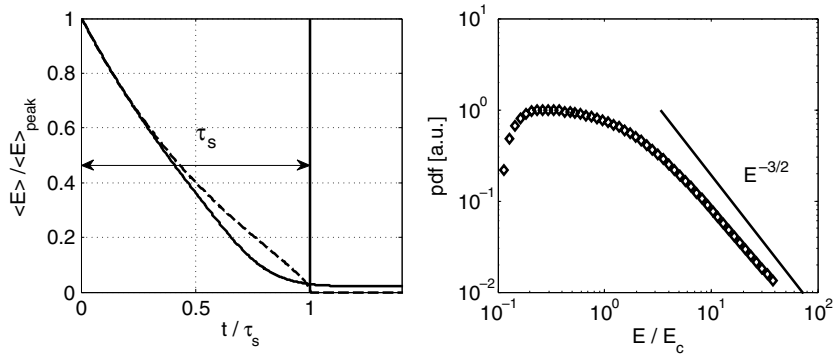

Figure 6. Mean energy distribution, as a function of time, for an isotropic distribution of deuterium ions (left panel). The numerical results (solid line) are compared with the theoretical prediction of equation (8) (dashed line). The slowing down distribution of a similar ensemble of numerical particles exhibits long energy tails consistent with the expected power law decay of equation (7) (right panel).

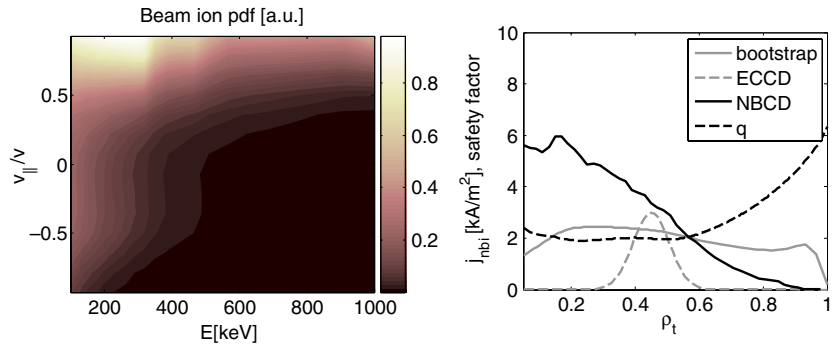

Figure 7. Distribution function of neutral beam ions, generated by the beam ionization model described in section 3, as a function of energy and pitch angle (left panel). The pitch angle scattering expected for lower energy ions is evident for $E < E_c$. The beam driven current calculated by the VENUS code closely resembles the beam deposition profile shown in figure 5 (right panel).

angle ξ. As these particles approach $E_c \simeq 500\,\text{keV}$ (in the central region) they interact more importantly with the background ions. As a consequence, we observe a distinct broadening of the pitch angle distribution. The injection of particles at fractional energies $E_{\text{nbi}}/2$ and $E_{\text{nbi}}/3$ is also noticeable in the figure. The current profile generated by such distribution can be observed in the same figure. The similarity between the driven current profile and the beam deposition profile of figure 5 is observed, confirming the assumptions made in the previous section. It should be noted that the beam driven current is proportional to the drag coefficient described in [28]. Also illustrated in the figure is the safety factor profile calculated by the CHEASE code by adding the bootstrap and ECCD current to the NBCD component. The key features of the steady-state scenario have been reproduced correctly.

4. Anomalous redistribution of the NBCD profile

In the last part of the analysis we assess the influence of anomalous diffusion over the neutral beam driven current. We observed in section 2.2 the complexity of the anomalous diffusion

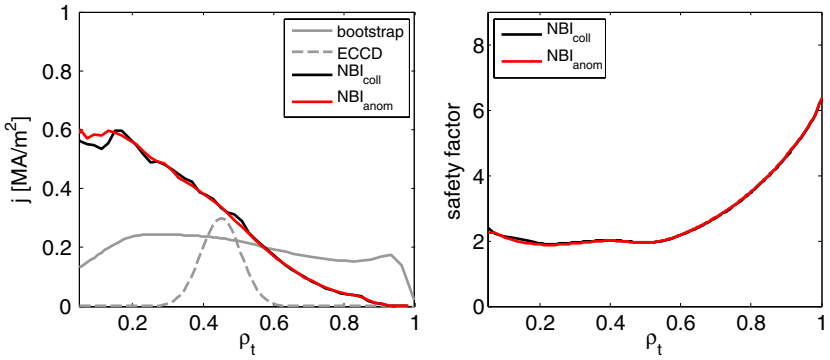

Figure 8. Neutral beam driven current density profile (left panel) for the collisional case (solid black line) and the anomalous model of equation (9) (solid red line). The bootstrap and ECCD current density profiles are also shown (solid and dashed grey lines, respectively). The corresponding modifications to the safety factor profiles as calculated by the CHEASE code are illustrated in the right panel.

coefficient of NBI particles, with a strong dependence on energy, pitch angle and poloidal location. Our model is based on a local approximation, such that radial dependences, observed in [10], cannot be reproduced. We can nevertheless define a global particle diffusivity as follows:

$$D_{\text{anomalous}}(\boldsymbol{x}, \xi, E) = D_1(\rho_t) \times D_2(\xi, E, \theta), \tag{9}$$

assuming toroidal symmetry. The variable D_2 is extracted in the form of a numerical matrix from the nonlinear simulations performed with the GENE code. The Monte-Carlo scheme employed to model the anomalous diffusive process interpolates the numerical diffusivity D_2 at the particle position. For simplicity, we choose a Gaussian radial envelope with $\sigma/a = 0.25$ as the function D_1.

The results of the numerical simulation of the NBCD profile redistribution are illustrated in figure 8. Contrary to the results of figure 4, only a small change in the NBCD profile is observed in this scenario. We can explain this result by considering the low diffusivity of particles in the velocity space region close to the injection energy, where a substantial fraction of the beam current is driven. Particles experiencing larger diffusivities are located in the low energy region where contributions to the current profile are small. The largest modification to the NBCD profiles is found in the plasma core region, where our model is less accurate given the assumption of a Gaussian radial envelope for the particle diffusivity. Smaller differences are observed at the mid-radius region, where the model is more precise as the flux tube simulations have been performed at $\rho_t = 0.5$.

In figure 8 we show the safety factor variation corresponding to the redistribution of the beam driven current, as calculated by the CHEASE code. A similarly small modification to the safety factor profile is observed. These negligible modifications therefore justify the choice of a tracer model, where the equilibrium is not recomputed when j_{nbi} changes. More detailed models, similar to those described in [29, 30], would be envisaged for a more accurate and self-consistent treatment of experimental scenarios.

We can conclude that the consequences in terms of transport and confinement features are apparently limited in this configuration. The stability of the plasma column, which is one of the main advantages of advanced scenarios [6], could be affected if lower energy neutral beams are employed, as demonstrated in the following section.

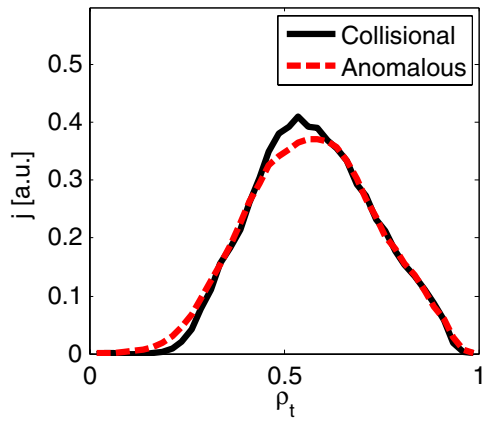

Figure 9. Neutral beam driven current density profile for a collisional case (solid black line) and the anomalous model of equation (9) (dashed red line). The anomalous redistribution of the NBCD profile during off-axis deposition of low energy ions is more significant than for a high energy on-axis deposition.

4.1. Low energy NBI and off-axis deposition

Only a minor beam ion redistribution was observed in the results of the previous section, mainly due to the small diffusivity of the beam particles near the birth energy. A lower energy NBI, on the other hand, would be affected more strongly by the microturbulent fields. It has been shown that lower values of the ratio E_b/T_e cause larger beam anomalies [9, 10, 12]. We can test this assumption by lowering the beam injection energy to 300 keV. At the same time, we move the NBI deposition off-axis at $\rho_t = 0.5$, where our model is the most accurate. The corresponding value of $E_b/T_e = 20$ would be smaller that the value in the case of high energy deposition by a factor 3 at mid-radius. The results of figure 9 indicate that the redistribution of the NBCD is more important in this configuration, consistent with our expectations. The lower beam injection generates particles in the velocity space region where anomalous transport is more intense than in the on-axis case. A final observation can be made on the ratio of the beam injection energy and the plasma temperature $E_b/T_e = 20$. This value is roughly the same achieved in present day tokamaks. In particular, recent experiments in ASDEX Upgrade [11] were characterized by similar off-axis beam deposition and redistribution. Our results suggest that the anomaly was caused by microturbulence, in agreement with the findings of [8, 9, 31].

5. Conclusions

In this work we have studied the interaction between energetic ions created by neutral beam injection and microturbulent fields. We simulated the small scale turbulence characterizing the ITER steady-state scenario with the GENE code. Linear simulations first unveiled the fundamental properties of the microinstabilities generating the background turbulence in this plasma configuration. Nonlinear simulations were then performed, including a high energy distribution of deuterium ions. The results indicate that the transport of these particles can become important, especially for passing ions at energies of the order of 100 keV.

The NBCD profile in ITER was studied with the single particle following code VENUS. At first we included the effect of unperturbed particle drifts and collisions for an arbitrary beam line geometry. A broad NBCD profile was observed and the flat safety factor profile distinctive

of the ITER steady-state scenario was generated. The anomalous diffusivity extracted from the GENE code was then introduced in the VENUS code and the beam driven current recalculated. The inclusion of microturbulent transport caused a small reduction in the NBCD current in the core. Similar minor modifications to the flat safety factor profile envisaged for the ITER steady-state scenario were observed. Major changes to the beam driven current were observed when employing a lower energy off-axis NBI. More important consequences in terms of plasma stability would therefore be expected in such a configuration.

Further investigation with more detailed models will clarify the accuracy of the model employed in this work. In particular, global gyrokinetic simulations for a precise description of the radial dependence of the turbulent fields will be performed. This will enable a complete investigation of the consequences in terms of equilibrium properties and transport features of this important plasma configuration.

Acknowledgments

The authors gratefully acknowledge fruitful discussions with S Brunner, F Jenko and L Villard. This work was partly supported by the Swiss National Science Foundation. The simulations have been run on the Pleiades2 cluster at the Ecole Polytechnique Fédérale de Lausanne (EPFL) and on the HPC-FF cluster at the Jülich Supercomputing Center (JSC).

References

[1] Fasoli A *et al* 2007 *Nucl. Fusion* **47** S264
[2] Wade M R *et al* 2007 *Nucl. Fusion* **47** 543
[3] Oyama N *et al* 2009 *Nucl. Fusion* **49** 104007
[4] Romanelli F *et al* 2009 *Nucl. Fusion* **49** 104006
[5] Meyer H *et al* 2009 *Nucl. Fusion* **49** 104017
[6] Gormezano C *et al* 2007 *Nucl. Fusion* **47** 285
[7] Estrada-Mila C *et al* 2006 *Phys. Plasmas* **13** 112303
[8] Dannert T *et al* 2008 *Phys. Plasmas* **15** 062508
[9] Hauff T *et al* 2009 *Phys. Rev. Lett.* **102** 075004
[10] Zhang W *et al* 2008 *Phys. Rev. Lett.* **101** 095001
[11] Günter S *et al* 2007 *Nucl. Fusion* **47** 920
[12] Heidbrink W *et al* 2009 *Phys. Rev. Lett.* **103** 175001
[13] Albergante M *et al* 2009 *Phys. Plasmas* **16** 112301
[14] Angioni C *et al* 2009 *Nucl. Fusion* **49** 055013
[15] Angioni C *et al* 2008 *Phys. Plasmas* **15** 052307
[16] Jenko F *et al* 2000 *Phys. Plasmas* **7** 1904
[17] Fischer O *et al* 2002 *Nucl. Fusion* **42** 817
[18] Lütjens H *et al* 1996 *Comput. Phys. Commun.* **97** 219
[19] Kammerer M *et al* 2008 *Phys. Plasmas* **15** 052102
[20] Lapillonne X *et al* 2009 *Phys. Plasmas* **16** 032308
[21] Pueschel M J *et al* 2008 *Phys. Plasmas* **15** 102310
[22] Candy J 2005 *Phys. Plasmas* **12** 072307
[23] Görler T *et al* 2008 *Phys. Rev. Lett.* **100** 185002
[24] Albergante M *et al* 2010 *Nucl. Fusion* **50** 084013
[25] Wesson J A 2004 *Tokamaks* (Oxford: Clarendon Press)
[26] Suzuki S *et al* 1998 *Plasma Phys. Control. Fusion* **40** 2097
[27] Boozer A H *et al* 1981 *Phys. Fluids* **24** 851
[28] Graves J P *et al* 2010 *Nucl. Fusion* **50** 052002
[29] Barnes M *et al* 2010 *Phys. Plasmas* **17** 056109
[30] Jucker M *et al* 2011 *Plasma Phys. Control. Fusion* **53** 054010
[31] Hauff T *et al* 2008 *Phys. Plasmas* **15** 112307